Radium sorption on biotite; surface complexation modeling study

Fabritius, Otto

2022-05

Fabritius , O , Puhakka , E , Li , X , Nurminen , A & Siitari-Kauppi , M 2022 , ' Radium sorption on biotite; surface complexation modeling study ' , Applied Geochemistry , vol. 140 , 105289 . https://doi.org/10.1016/j.apgeochem.2022.105289

http://hdl.handle.net/10138/344439
https://doi.org/10.1016/j.apgeochem.2022.105289

Applied Geochemistry 140 (2022) 105289

Contents lists available at ScienceDirect

Applied Geochemistry

journal homepage: www.elsevier.com/locate/apgeochem

Radium sorption on biotite; surface complexation modeling study

Otto Fabritius *, Eini Puhakka, Xiaodong Li, Anita Nurminen, Marja Siitari-Kauppi

Department of Chemistry, University of Helsinki, P.O. Box 55, FIN-00014, Finland

ARTICLE INFO

Editorial handling by Dr J Lützenkirchen

Keywords:
Radium
Sorption
Biotite
Nuclear waste
Deep geological disposal
PHREEQC

ABSTRACT

The sorption of Ra on Olkiluoto biotite in the context of deep geological disposal of spent nuclear fuel was studied with isotherm batch sorption experiments. Ba was used as an analog for Ra in the experiments and modeling studies. A wide concentration range of Ra/Ba was used in the isotherm studies (2.6×10^{-9} M to 1×10^{-3} M) in addition to four different Olkiluoto reference groundwaters with salinity types ranging from fresh to saline. Experimental results show that both in the fresh and saline reference groundwaters, the distribution coefficients of Ra tend to decrease in the higher isotherm concentrations of Ba. With one reference groundwater, the distribution coefficients increased with the concentration of Ba due to significant coprecipitation of Ra. With the fresh reference groundwaters, the distribution coefficients of Ra were consistently approximately one order of magnitude lower than in the saline reference groundwater. A PHREEQC multi-site complexation model coupled with an optimization tool in Python was used to interpret the experimental Ra sorption results. Molecular modeling with CASTEP code implemented into Materials Studio was used to update the PHREEQC model with more realistic biotite sorption site density data. It was observed that while the multi-site model predicts the sorption of Ra well in lower isotherm concentrations, auxiliary reactions of Ra disrupt the model in high Ba isotherm concentrations. The experimental and modeled distribution coefficient data of Ra on biotite can be used in the safety case calculations of the deep geological disposal of spent nuclear fuel in Finland and Sweden.

1. Introduction

Spent nuclear fuel from the Finnish nuclear power plants of Olkiluoto and Loviisa will be permanently disposed of in an underground repository facility in Olkiluoto, Finland (Posiva, 2012a, 2012b, 2013; Hellä et al., 2014; Ervanne et al., 2014; Jonsson et al., 2018). As a part of the legislated responsibility of the disposal authority in Finland, Posiva, a safety case study concerning the disposal site and the migration of the nuclear waste borne radionuclides has been commissioned (Posiva, 2012b, 2017; Hellä et al., 2014). The KBS-3 principle of the disposal facility is to provide multiple barriers, both natural and engineered, to minimize the possibility of escape and further transport of the radionuclides from the waste containment (Posiva, 2012b).

After the first engineered retentive barriers, the final protection against the spread of the harmful waste-borne radionuclides is the stable crystalline rock surrounding the underground disposal facility. Thus, understanding the whole system of the bedrock matrix is of importance for the safety considerations of the disposal process. To this end, several key parameters of the crystalline rock in the disposal test sites have been studied extensively: porosity of the rock matrix and fracturation of Olkiluoto rocks (Kuva et al., 2012; Sammaljärvi et al., 2017), advection and flow properties with gas (Kuva, 2016) and in the water phase (Voutilainen et al., 2019), diffusion (Voutilainen et al., 2016, 2018; Aromaa et al., 2019), and sorption (Ervanne et al., 2014; Muuri et al., 2016, 2017; Söderlund et al., 2019). Furthermore, the matrix diffusion (Neretnieks, 2013; Tsang et al., 2015), flow (Liu et al., 2018; Neretnieks and Winberg-Wang, 2019), and advection (Shahkarami et al., 2015) of radionuclides in saturated rock and rock fractures have been reported previously. Finally, the sorption of radionuclides has been assessed by the Finnish and Swedish spent nuclear fuel disposal authorities Posiva and SKB, respectively, in the form of distribution coefficient studies as a part of the safety case calculations of the spent nuclear fuel disposal facility (Crawford, 2010; Posiva, 2013).

In the Finnish safety case calculations, ^{226}Ra is recognized as one of the safety relevant radionuclides in the context of deep geological disposal due to its importance as one of the three main dose contributing radionuclides (Posiva, 2021; Mäki, 2021). Additionally, the Swedish safety case calculations argue that ^{226}Ra must be considered a high priority waste nuclide due to its enrichment in the waste as a decay daughter of ^{238}U, and due to its notable potential for mobility in the

* Corresponding author.
E-mail address: otto.fabritius@helsinki.fi (O. Fabritius).

https://doi.org/10.1016/j.apgeochem.2022.105289
Received 14 October 2021; Received in revised form 11 February 2022; Accepted 29 March 2022
Available online 31 March 2022

geosphere (SKB, 2006; Crawford, 2010; Jaremalm et al., 2013). As $^{238}UO_2$ is the main component of spent nuclear fuel, the radioactive progeny of ^{238}U is of special interest when considering the safety issues of the spent nuclear fuel disposal. As a decay daughter of ^{238}U, ^{226}Ra has a notable significance in the near and far-field dose rate assessments of the nuclear fuel disposal safety case (Crawford, 2010; Ervanne et al., 2014; Mäki, 2021). This significance has been, in part, concluded in the safety case calculations in which ^{226}Ra is the primary contributing radionuclide of the main dose in the growing pinhole containment failure scenario after 50,000 years of repository lifetime (Grandia et al., 2008). In 300,000 years of disposal lifetime, the activity of ^{238}U-borne ^{226}Ra in an individual KBS-3 canister reaches its maximum of 8.6–9.3 × 10^{10} Bq, depending on the contained fuel type (SKB, 2006; Grandia et al., 2008).

In addition to being an important spent nuclear fuel borne radionuclide, ^{226}Ra is classified as a Naturally Occurring Radioactive Material or NORM. Isotopes of Ra occur in the three major natural decay chains of ^{235}U, ^{238}U, and ^{232}Th, in the form of ^{223}Ra, ^{226}Ra, and ^{228}Ra and ^{224}Ra, respectively. Of these, ^{226}Ra, with a half-life of 1600 a, is the most abundant isotope in the Earth's crust (IAEA, 2014). Radium-226 decays via alpha decay into ^{222}Rn, a widely known gaseous radionuclide that causes more than 50% of the average annual effective dose of the population of Finland (Muikku et al., 2014). Radium is found in areas of uranium-rich rocks, where Ra is Outleached [sic] from the host rock and soil by rainfall and the surrounding groundwater (Greeman et al., 1999; Breitner et al., 2008; IAEA, 2014). Radium can also pose environmental problems in areas where U ore is mined and processed. Outdoor storages of U mining mill tailings are at risk of leaching out Ra due to rainfall or residual acid drainage from the ore processing (Martin et al., 2003; IAEA, 2004, 2014; Déjeant et al., 2014).

Should the containment of the spent nuclear fuel fail due to canister corrosion or damage, and the waste come in touch with groundwater, waste radionuclides are in danger of being released from the fuel matrix. Ewing (2015) discusses both the fast and the slow release of waste nuclides: fission product gases, such as Xe and Kr, and volatile elements, such as I, Cs, and Cl, are released instantaneously from the waste, whereas the heavy metal radionuclides, such as $^{235,238}U$, are slower to release. The long-term release processes of U can be summarized as a combination of U oxidation from U(IV) to U(VI) and the subsequent complexation and hydrolysis with intruding water, bulk dissolution of the fuel UO_2, and the formation of other alteration products such as coffinite, $U(SiO_4)_{1-x}(OH)_{4x}$ (Ewing, 2015).

Radium is part of the alkaline earth metal group and exists solely in the oxidation state of Ra(II). Radium often forms readily soluble compounds. Exceptions to this tendency of soluble compounds are $RaCO_3$ and $RaSO_4$, which are only moderately and very sparingly soluble, respectively (Lehto and Hou, 2011). The sorption behavior of Ra has been studied before in, e.g., minerals such as goethite, ferrihydrite, and barite (Sajih et al., 2014; Vinograd et al., 2018), rapakivi granite crystalline rock (Huitti et al., 1996), early cretaceous clays (Missana et al., 2017), and artificial materials such as cement (Olmeda et al., 2019). As Ra has no stable isotopes, the next heaviest alkaline earth metal Ba has often been used as an analog for Ra in studies due to radiation safety issues and convenience (Matyskin, 2018; Muuri et al., 2018; Söderlund et al., 2019). The ionic sizes (Ra^{2+} r_{ion}(coordination 8) = 1.62 Å, r_{ion}(coordination 12) = 1.84 Å, and Ba^{2+} r_{ion}(coordination 8) = 1.56 Å, r_{ion}(coordination 12) = 1.75 Å) (Shannon, 1976) and chemical properties of the Ra and Ba, though highly similar, cause slight differences in solubilities and crystal structures between some compounds of the two elements (Matyskin et al., 2017; Matyskin, 2018). Barium was used in this study as an analog for Ra in the batch sorption experiments and sorption modeling.

The aim of this work was to: 1) determine distribution coefficients of Ra sorption on biotite in different reference groundwater conditions to provide data for the deep geological disposal safety case calculations; 2) examine the sorption mechanisms of Ra using the Ba/Ra concentration isotherm in the batch sorption experiments and; 3) interpret the experimental distribution coefficient results with the PHREEQC geochemical computer model supported by Density Functional Theory (DFT) sorption site density calculations.

2. Materials and methods

2.1. Geology and mineralogy of the Olkiluoto site

The Olkiluoto nuclear site lies on the island of Olkiluoto, located in southwestern Finland on the coast of the Baltic Sea. Olkiluoto lies in the Southern Svecofennian complex geological area, where the land is still in the post-glacial uplifting phase, rising approximately 6 mm annually (Posiva, 1996; Aaltonen et al., 2016).

Olkiluoto site's bedrock is often divided into four main series with the three most prevalent named T, S, and P-series, respectively (Kärki and Paulamäki, 2006; Aaltonen et al., 2016). The T-series consists mainly of metatexites and diatexites with mica and quartz gneisses, and tonalite-granodiorite-granite gneisses. The S-series consists of mafic gneisses and quartz gneisses with high levels of calcium from calcareous sediments. The P-series is made up of granodioritic and tonalitic tonalite-granodiorite-granite gneisses with high levels of phosphorus. At the planned disposal depth of the Olkiluoto site, the main rock type is veined gneiss (Kärki and Paulamäki, 2006). The phyllosilicate mineral biotite is one of the main minerals in veined gneiss, and can make up to 40% of the total mass of the host rock (Lindberg, 2001; Kärki and Paulamäki, 2006). Due to the prevalence of biotite in the Olkiluoto site's bedrock, it was chosen for this study as the solid phase of batch sorption experiments.

2.2. Hydrogeochemical conditions of Olkiluoto and the choice of groundwater simulants

Olkiluoto site consists of groundwater layers in which groundwater types and salinity vary with depth. As Olkiluoto is an island, the hydrogeological changes of the surrounding Baltic Sea have affected the groundwater chemistry. The effects of the ancient Litorina Sea (8000-2500 BP) are still observed in modern times in the hydrogeochemistry of the Olkiluoto site: redox conditions are anoxic in groundwaters from few meters depth below groundwater table, and additionally there exists a band of heightened sulfate and magnesium levels at the depth of 100–300 m (Posiva, 2012c). Indeed, groundwater SO_4^{2-} levels as high as 500–600 mg l^{-1} have been observed at the depth of 100–300 m in Olkiluoto (Posiva, 2012c; Partamies and Pitkänen, 2014). However, sulfate was limited at the depth of 300 m at the baseline conditions before the construction of the disposal facility started, and it does not occur at the planned repository depth of 400–500 m (Posiva, 2012c). At the Olkiluoto site groundwaters, the natural concentration of stable Ba has been reported to vary from 5.9 × 10^{-7} to 1.9 × 10^{-5} M (Hellä et al., 2014). The natural concentrations of Ra in Finnish groundwaters vary most commonly between 10^{-14} to 10^{-11} M (Vaaramaa et al., 2003).

To categorize the different types of groundwater in Olkiluoto, the Total Dissolved Solids (TDS) classification of Davis (1964) has been used (Posiva, 2012c). According to the classification, the Olkiluoto site groundwaters are divided into three categories based on the amount of TDS in them in g l^{-1}: fresh TDS <1 g l^{-1}, brackish 1 g l^{-1} < TDS <10 g l^{-1}, and saline 10 g l^{-1} < TDS <100 g l^{-1}. In Olkiluoto, at the depths of 60 m to 400–500 m, the groundwater is reported as 'brackish' with TDS ranging between 2 and 9.8 g l^{-1} with two distinct types of groundwater identified: bicarbonate-rich layer down to the depth of 100–150 m and the sulfate-rich Litorina-type water at depths of 100–300 m (Vuorinen and Snellman, 1998; Posiva, 2012c). From there, the salinity of the groundwater rises steadily with the increasing depth: 10–70 g l^{-1} between 400 and 800 m, and 130 g l^{-1} at 900 m from the surface (Posiva, 2012c). The salinity of Olkiluoto groundwaters is most commonly the result of high amounts of Na, Ca, and Cl in the waters, and the relative

fraction of Ca increases with salinity (Vuorinen and Snellman, 1998; Vieno, 2000; Posiva, 2012c). In the context of deep geological disposal and the safety case calculations, the salinity of the surrounding groundwater is crucial, as highly saline water can damage the waste containment architecture and hinder the safety procedures. Additionally, as shown in literature, highly saline water conditions can result to decreased sorption of Ra and Ba, among other elements, onto the crystalline rock and its minerals, possibly encouraging further migration of these nuclear waste borne radionuclides in the lithosphere (Huitti et al., 1996; Sajih et al., 2014; Muuri et al., 2018; Söderlund et al., 2019).

Because of the different groundwater layers the migrating Ra will be facing in the case of a containment breach in the disposal facility, four Synthetic Ground Waters (SGW) of different TDS salinity types and chemical compositions were chosen for this study. The chosen SGWs were: 'fresh' mildly reducing ALLMR, a modification of the commonly used Allard granitic reference groundwater; 'saline' reducing OLSR; 'fresh' glacial meltwater OLGA; and the carbonate and sulfate containing 'brackish' OLBA (Hellä et al., 2014; Söderlund et al., 2019). The ionic compositions of the chosen reference groundwaters are presented in Table 1.

2.3. Biotite and sample preparation for batch sorption experiments

Biotite, $K(Mg,Fe)_3AlSi_3O_{10}(OH,F)_2$, belongs to the group of phyllosilicates which are formed by superposed atomic planes parallel to the (001) face of the crystalline structure (Velde and Meunier, 2008). They have a prismatic and sheet-like structure, where cation layers connect the negatively charged layers to each other. The negatively charged layers consist of tetrahedral (T) and octahedral (O) sheets that stack together to form 2:1 (TOT) layers with a characteristic repeat distance between them (Viani et al., 2002). The negative framework charge is balanced by an equivalent amount of cations on the internal and external basal planes and these ions are readily exchangeable to ions in external solutions. In the modeling phase in this work, the biotite surface is assumed neutral.

Crushed biotite obtained from the Olkiluoto site (Geological Survey of Finland) was chosen for this study. The biotite was milled and sieved to the grain size of 0.071–0.3 mm. The mineralogy of the biotite was confirmed as mainly phlogopite with the X-Ray Diffraction (XRD) at the Geological Survey of Finland. The Specific Surface Area (SSA) was determined at the Chalmers University of Technology with the Kr-BET method using gas adsorption analyzing instrument (Micromeritics ASAP2020).

To try to convert the biotite sheet edge surfaces into the monopotassium form used in the modeling, the biotite sample was pretreated with analytical grade $KClO_4$ to exchange Ca and Na impurities with K from biotite surface's sorption sites as further specified in (Armarego and Chai, 2012; Li et al., 2020). Fifty grams of the crushed biotite sample was packed into a glass cation exchange column and 0.1 M $KClO_4$ was pumped through the column with a peristaltic pump at the flow rate of 4 ml h^{-1} for two weeks. Finally, for the last two days of wash, 0.01 M $KClO_4$ and MilliQ-water were pumped through the column to remove excess K. After the $KClO_4$ pretreatment, the biotite sample was dried in a vacuum oven overnight.

Table 1
The ionic compositions (mg/l) of the Olkiluoto reference groundwaters used in the experiments, along with the set pH and the reference ionic strengths (I) (Hellä et al., 2014; Söderlund et al., 2019).

Ion	Concentration of the ion or substance (mg/L)			
	ALLMR	OLSR	OLGA	OLBA
Na^+	52.5	4800	0.66	1750
K^+	3.9	21	0.6	18.9
NH_4^+	–	–	–	0.33
Mg^{2+}	0.7	54.6	0.3	26.5
Ca^{2+}	5.1	4000	0.52	84.5
Sr^{2+}	–	35	–	0.1
$B(OH)_3$	–	5.3	–	3.5
Cl^-	48.8	14,500	3	2530
HCO_3^-	165	–	–	111
SiO_2	17	–	0.1	6.1
SO_4^{2-}	9.6	4.2	0.2	458
F^-	–	1.2	–	0.3
I^-	–	0.9	–	–
Br^-	–	104.7	–	13.1
pH	8.8	8.3	5.8	7.6
I (mmol/l)	4.31	515	0.123	91.4

2.4. Batch sorption experiments

The batch sorption experiments were done at room temperature in a regular atmosphere ventilated glove box. To study the effect of salinity on the sorption of Ra, four different reference groundwater simulants of varying salinity were used. To examine the sorption mechanisms of Ra, and to provide data for the sorption modeling, a broad concentration isotherm range of Ba/Ra between 2.3×10^{-9} M to 1×10^{-3} M was chosen for the experiments. The lower part of the concentration range thus represents close to natural levels of concentration of Ba in Finnish groundwaters (10^{-9} to 10^{-5} M) (Vaaramaa et al., 2003; Posiva, 2012c; Ervanne et al., 2014). The high end of the employed concentration scale was chosen to study the effect of significant mineral sorption site saturation on the sorption of Ra. Since Ra has no stable isotopes, using pure Ra for the isotherm studies would have been infeasible in terms of radiation safety concerns. Hence, inactive Ba was used as an analog for Ra to set the concentration isotherm in the experiment.

The milled and sieved $KClO_4$ pretreated biotite samples were agitated for three weeks with the groundwater simulants in 20 ml low diffusion polyethylene liquid scintillation vials, with a solid-to-solution ratio of 50 g l^{-1} (0.5 g of biotite and 10 ml of SGW). After the initial equilibration of biotite and the SGW, the samples were first spiked with Ba ($BaCl_2$, Merck) to create the desired concentration isotherm, and subsequently with the radiotracer of ^{226}Ra ($^{226}Ra(NO_3)_2$ in 1 M HNO_3 with 10 μg l^{-1} Ba carrier, Eckert & Ziegler). Note that at the lowest isotherm concentration conditions, no $BaCl_2$ was added to the solutions as just the spiked ^{226}Ra tracer caused the desired concentration. The amount of added radiotracer corresponded to approximately 200 Bq of ^{226}Ra. After this, the samples were further agitated for three weeks. Due to the observations of previous sorption studies (Muuri et al., 2018; Söderlund et al., 2019), it was concluded that the sorption solutions would not need to be pH buffered, but instead let be equilibrated with the minerals and atmosphere for the duration of the experiment. The pH of selected sorption samples from each concentration conditions were measured immediately after the second agitation period with the reference water, biotite, and spiked Ba and ^{226}Ra, after sorption solution supernatant sampling for the activity measurements.

After the second agitation, the samples were centrifuged (3×10 min, 3000 rpm with Sigma 3–16 KL) and an aliquot of 5 ml of the supernatant sample was pipetted into 20 ml polyethylene liquid scintillation vials. The activity of the supernatant ^{226}Ra was measured from the 186.2 keV (intensity 3.64%) gamma peak with an HPGe gamma-ray detector (Canberra Semiconductor Detector, GX8021) with measurement times of 1 h–5 d depending inversely on the magnitude of activity of the samples, which varied from 1 Bq to over 100 Bq. Due to the high amount of tested sorption samples, the gamma measurement approach was chosen for this study to avoid the laborious pretreatment requiring and high amounts of radioactive waste producing liquid scintillation counting and mass spectrometry methods. The Minimum Detectable Activity (MDA) for ^{226}Ra in the chosen gamma counter measurement setup of the 5 ml measurement geometry was calculated to be 0.2 Bq ml^{-1}. To control the accuracy of the measured ^{226}Ra activity, the activities of ^{226}Ra decay daughters ^{214}Pb (gamma emission of 351.9 keV, intensity 35.6%) and ^{214}Bi (gamma emission of 609.3 keV, intensity 45.49%) in selected supernatant samples were measured again with

gamma-ray detection after three weeks of activity equilibration in hermetically sealed vessels. The activities of the ^{226}Ra decay daughters ^{214}Pb and ^{214}Bi, with MDAs in the used gamma counting setup being 0.012 Bq ml^{-1} and 0.008 Bq ml^{-1}, respectively, were observed to be in good agreement with the initially measured ^{226}Ra activities. Thus, the interference from the measurement room background radiation ^{235}U gamma peak of 185.7 keV (intensity 57%) on the ^{226}Ra activity gamma-ray measurement was determined to be small. Background ^{235}U gamma emissions of the measurement setup were further taken into account in the MDA of ^{226}Ra as a part of the activity background calculations.

The distribution coefficient K_d of Ra on the investigated biotite was calculated with Eq. (1):

$$K_d = \frac{A_i - A_f}{A_f} \times V \Big/ m \quad (1)$$

where A_i is the initial activity of the spiked ^{226}Ra; A_f is the activity of ^{226}Ra left in the groundwater supernatant after agitation; V (ml) is the volume of the reference groundwater, and m (g) the mass of the biotite solid phase in the batch sorption samples. Radium adsorption loss onto laboratory equipment during the agitations and analysis procedures was taken into account in term A_f.

2.5. Molecular modeling

Molecular modeling was used to justify the sorption behavior of Ra onto biotite in the sorption modeling. Biotite mineral has two end-members: phlogopite and annite, with phlogopite being a common form of biotite in the Olkiluoto area and thus used in the experimental part of this study. The molecular modeling was done on the Mg-rich phlogopite, $KMg_3(AlSi_3O_{10})(OH)_2$, where all the Fe ions of biotite have been substituted by Mg. Fe, or Mg, do not have a role in the sorption of Ra in this context. As such, Fe and the elemental impurities of the K^+ cationic layer sheet edge were excluded to simplify the molecular modeling calculations. The calculations were performed for the periodic system using the density functional CASTEP (CAmbridge Serial Total Energy Package) code implemented into Materials Studio version 6.0. As for the phlogopite systems, the calculations were done using the CASTEP code implemented into Materials Studio version 2020 (Dassault Systèmes, 2019). The exchange-correlation was described with generalized gradient approximation GGA-PBE. As a compromise between the accuracy and computational time of calculations, the ultrasoft pseudopotentials were used for each element. The used potentials were Al_00PBE.usp for Al, Ba_00PBE.usp for Ba, Cs_00PBE.usp for Cs, H_00PBE.usp for H, K_00PBE.usp for K, Mg_00.usp for Mg, O_soft00.usp for O, Ra_00.usp for Ra, Si_soft00.usp for Si and Sr_00PBE.usp for Sr. The kinetic cut-off energy for a plane wave expansion of the wave function was 310 eV.

2.6. Sorption modeling

To interpret the experimental sorption results, the geochemical modeling software PHREEQC was used. PHREEQC is one of the most widely used modeling tools for geochemical applications in aqueous, mineral and gas conditions (Parkhurst and Appelo, 2013). In this study, a model derived from the multi-site sorption model of Bradbury and Bayens (2000) was used to describe the sorption of Ba as a well-defined analog of Ra on the surface of biotite in the varying Ba concentrations. The multi-site sorption model has previously been adapted for alkaline earth metal sorption studies by, e.g., (Muuri et al., 2017, 2018). The thermodynamic database of Lawrence Livermore National Laboratory (LLNL) was used in the PHREEQC sorption modeling.

Ion exchange properties of the biotite mineral sheet edge outer K^+ were taken into consideration in the model. In PHREEQC modeling, cation exchange sorption processes can be described as binary ion exchange reactions according to the Gaines-Thomas convention (Appelo and Postma, 2005):

$$M - K + 1/2\ Ba^{2+} \leftrightarrow 1/2\ Ba - M_2 + K^+$$

where the cation exchange sites (M^-) are initially filled with K^+ of the biotite cationic intermediate layers.

To characterize the surface complexation part of Ba sorption on biotite as a function of barium concentration from 10^{-9} to 10^{-3} M, a Dzombak and Morel diffuse double layer model based approach was used (Dzombak and Morel, 1990; Li et al., 2018). Two types of surface complexation sorption sites on the neutral surface of biotite are employed in the PHREEQC model: strong sorption sites are expressed as (≡S_sOH) while the weak sites are denoted as (≡S_wOH) (Ervanne et al., 2013; Li et al., 2018). In terms of Ba surface complexation reactions, following reactions were considered:

$$S\_sOH + Ba^{2+} \rightleftharpoons S\_sOHBa^{2+} \quad Log\ K = -5.47$$

$$S\_wOH + Ba^{2+} \rightleftharpoons S\_wOBa^{2+} + H^+ \quad Log\ K = -5.85$$

where S_sOH and S_wOH represent the strong and weak sorption sites, respectively. Log K values of the given reactions are referenced from the LLNL database, used in the PHREEQC modeling.

The coprecipitation of Ra with the insoluble barium minerals of barite ($BaSO_4$) and witherite ($BaCO_3$), as $(Ba,Ra)SO_4$ and $(Ba,Ra)CO_3$, respectively, has been recognized as a significant sink of aqueous Ra^{2+} in the presence of Ba^{2+}, and SO_4^{2-} and CO_3^{2-} (Grandia et al., 2008; Matyskin, 2018). To simulate this auxiliary removal of Ra from the solutions, the precipitation of Ba as those minerals was allowed during the thermodynamic balancing of the sorption modeling. In addition, as the batch sorption experiments were conducted in oxic conditions, the sorption reactions were balanced with the dissolving atmospheric CO_2 in the PHREEQC models.

In the interpretation of the experimental sorption results, an optimization and model fitting tool that coupled PHREEQC with Python was used (Charlton and Parkhurst, 2011; Wissmeier and Barry, 2011; Parkhurst and Appelo, 2013). To use the optimization tool, PHREEQC code is coupled with the Python programming language via the Microsoft COM (component object model) version of PHREEQC, called IPhreeqc (Charlton and Parkhurst, 2011). In the sorption model optimization iterative process, the previously fitted parameters are recalculated after each subsequent calculation step. The iteration process seeks to find the best possible fit for the model on the experimental values based on the least-squares difference between the experimental and modeled data. Should no satisfactory fit be found, the optimization tool starts the fitting anew with different initial parameters.

3. Results and discussion

3.1. Biotite characteristics

According to the XRD analysis, the biotite used in the batch sorption experiments was iron-bearing phlogopite of 1M structure, with the next most abundant phase being chlorite-clinochlore. For clarity, the used phlogopite in the experimental part of this study will hence be referred to as biotite, unless the distinction is crucial. Additionally, trace amounts of quartz and albitic plagioclase feldspar were detected in the XRD analysis.

The SSA of the experimented biotite was determined to be 0.6675 ± 0.0147 m^2 g^{-1} with the Brunauer-Emmett-Teller theory (BET) method. Li and group (2020) have previously reported the Cation Exchange Capacity (CEC) of the biotite also used in this study as 12.64 ± 0.42 meq kg^{-1}, obtained with the ammonium acetate method.

3.2. Adsorption sites by molecular modeling

In the present study, molecular modeling was used to investigate

possible changes in surface structures caused by sorption. Studies were performed on the hydroxylated (110) surface of phlogopite, which is its typical edge surface. The first objective was to find out how the surface structure changes when K^+ on the Frayed Edge Site (FES) positions are exchanged with Ba^{2+} and Ra^{2+}. Results were compared to our earlier results of Ba by Muuri and group (2018).

In Fig. 1, the bonding geometry of the uppermost cations after the ion exchange on the hydroxylated (110) surface of phlogopite is shown based on the molecular modeling optimized structures. According to the results, the surface structure of the phlogopite does not depend on if the uppermost cation is Ba^{2+} or Ra^{2+}. The cations are bonded to four hydroxyl groups, so that the hydroxyl groups together with the cation (in the middle of the coordination sphere) form a planar quadrate coordination structure, the size of which is approximately 0.15 nm^2. This structure binds the parallel TOT layers more strongly to each other so that the distance between the layers varies from 0.29 nm to 0.33 nm. Because this distance is significantly shorter than the characteristic repeat distance between the layers in the bulk structure (~0.4 nm), it is an indication that surface complexation reactions happen, and the uppermost interlayer cations on the FES positions have a strong effect on the surface properties of phlogopite.

The second objective was to define the outer-sphere electrostatic complexation sorption positions after the Ra^{2+} or Ba^{2+} exchange with the outermost K^+ on the hydroxylated (110) surface, and to calculate sorption energies. To get a systematic series of sorption energies, calculations were also performed to K, Cs, and Sr. Surface complexation sorption was studied onto two edge sites of phlogopite: a cut surface and a frayed edge site (Fig. 2). The surface complexation sorption energies are listed in Table 2. The results indicate that there are noticeable differences in sorption energies between different sorption sites. Additionally, monovalent ions (K^+ and Cs^+) seem to favor the sorption sites on the cut surface area whereas divalent ions (Ba^{2+}, Ra^{2+} and Sr^{2+}) favor the FES positions.

Based on these results, there are 5.6 strong sites nm^{-2} on the FES and 5.6 weak sites nm^{-2} on the cut surface for surface complexation reactions. In addition to this, there are 4.2 sites nm^{-2} on the basal site for ion exchange reactions. The calculated site density data was used in the PHREEQC modeling in interpreting site information for the Ra surface complexation sorption calculations.

3.3. Distribution coefficients

In the batch sorption experiments, it was observed that Ra sorbed very well on biotite with the magnitude of sorption correlating closely to the overall salinity of the reference groundwaters. In three of the four tested reference groundwater series, namely the fresh mildly reducing granitic ALLMR, fresh glacial meltwater OLGA, and saline reducing OLSR, the distribution coefficients of Ra were observed to decrease with the increasing Ba isotherm concentration and inherent salinity of the reference groundwater. In the brackish carbonate and sulfate containing OLBA, the distribution coefficients of Ra were observed to increase with the increasing Ba concentration. The comparison of experimental and PHREEQC modeled distribution coefficient results of Ra sorption on biotite for ALLMR, OLGA, OLBA, and OLSR are shown in Fig. 3. PHREEQC optimized modeling parameters concerning the reference groundwaters ALLMR, OLGA, and OLSR are given in Table 3. Model interpretation of OLBA sorption results are not shown, since they fail to fit the experimental data due to the very high amount of Ra removal from the solutions via coprecipitation. In the lowest tested isotherm conditions of 2.6×10^{-9} M, where no $BaCl_2$ was added due to the desired concentration achieved solely with the spiked 200 Bq of ^{226}Ra, the distribution coefficients of Ra on biotite were 0.25 ± 0.09 m^3 kg^{-1}, 0.17 ± 0.02 m^3 kg^{-1}, 0.035 ± 0.005 m^3 kg^{-1}, and 0.014 ± 0.002 m^3 kg^{-1} for the experimented reference groundwaters ALLMR, OLGA, OLBA, and OLSR, respectively. For the ALLMR, OLGA, and OLSR reference groundwaters, the expected decrease of distribution coefficients in the higher Ba isotherm concentration conditions is observed in the experimental results at the Ba concentration of 1×10^{-3} M: 0.048 ± 0.020 m^3 kg^{-1}, 0.010 ± 0.002 m^3 kg^{-1}, and 0.006 ± 0.003 m^3 kg^{-1}, respectively. For the reference groundwater OLBA, the experimental distribution coefficient of Ra in the highest Ba isotherm concentration was calculated to be 0.035 ± 0.005 m^3 kg^{-1}. The pH values of the sorption samples tended to stabilize in the mildly acidic to neutral conditions: pH varied from 6.3 to 7.3 for selected ALLMR samples, 6.3 to 6.6 for OLGA, 6.1 to 6.4 for OLBA, and 6.4 to 6.8 for OLSR.

The experimentally observed decreasing distribution coefficient trend of ALLMR, OLGA, and OLSR with increasing isotherm concentration is consistent with the multi-site cation exchange model of Bradbury and Bayens (2000) and previous work with Ra, and Ba as its analog in sorption (Muuri et al., 2017, 2018; Söderlund et al., 2019). According to the model, the high sorption affinity FESs receive most of the sorption in lower concentrations. As the ionic competition for the sorption reactions is less intense due to the smaller amount of competition, Ra^{2+} can easily access the high affinity sorption sites. As the limited high affinity sites start to get saturated with increasing amounts of sorption competing ions in the sorption solutions of higher salinity, the sorption reactions continue in the more numerous but lower affinity Planar and secondary sorption sites. Since Ra^{2+} is a poor competitor in the sorption reactions due to its large size, smaller alkali metal and alkaline earth metal ions, such as Na^+ and Ca^{2+}, instead take its place on the mineral sheet edge's sorption sites. This observation is also supported by the DFT modeling results, according to which the sorption energies of the lighter ions are much smaller than with Ra^{2+}. In sorption solutions of high ionic strength, an increasing amount of Ra^{2+} is only able to compete for the lesser affinity sorption sites, or is altogether left in the groundwater as the competition for sorption sites favors the lighter and smaller ions. This correlation of distribution coefficients and reference groundwater salinity is also observed in the sorption behavior of Ra in the batch sorption experiments. The measured distribution coefficients of Ra on biotite are consistently, throughout the Ba isotherm,

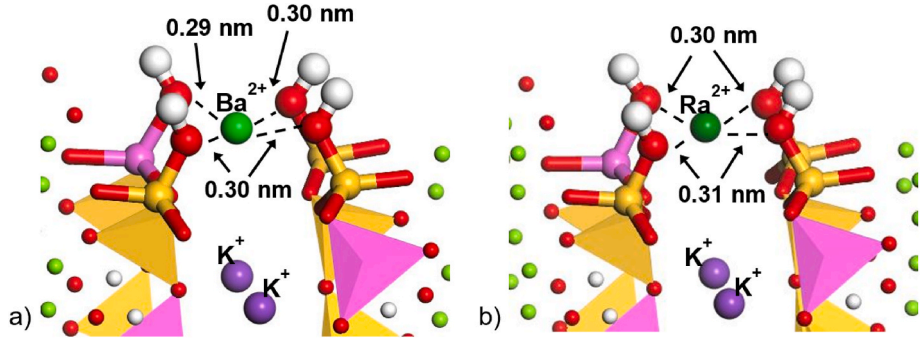

Fig. 1. The hydroxylated (110) surface of phlogopite. The uppermost K^+ ions are exchanged with a) Ba^{2+} and b) Ra^{2+} ions. Silicon: yellow. Aluminum: pink. Oxygen: red. Hydrogen: white. Magnesium: green. (For interpretation of the references to color in this figure legend, the reader is referred to the Web version of this article.)

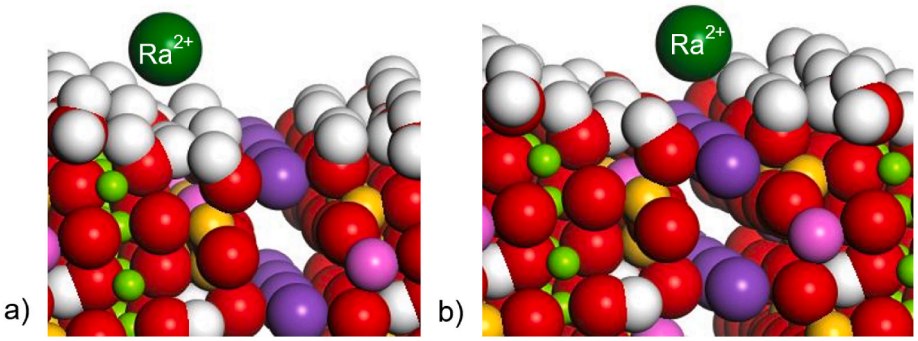

Fig. 2. The optimized surface complexation sorption positions of Ra^{2+} on two edge sites of phlogopite after outermost K^+ ion exchange: a) a cut surface and b) a frayed edge site. Aluminum – pink. Hydrogen – white. Magnesium – green. Oxygen – red. Silicon – yellow. Sodium – purple. (For interpretation of the references to color in this figure legend, the reader is referred to the Web version of this article.)

Table 2
Complexation sorption energies (eV) on the phlogopite (110) surface.

	Sorption site	
Ion	Cut surface	FES
K^+	−2.76	−2.40
Cs^+	−2.47	−2.13
Ba^{2+}	−6.39	−6.78
Ra^{2+}	−6.65	−6.90
Sr^{2+}	−7.54	−7.94

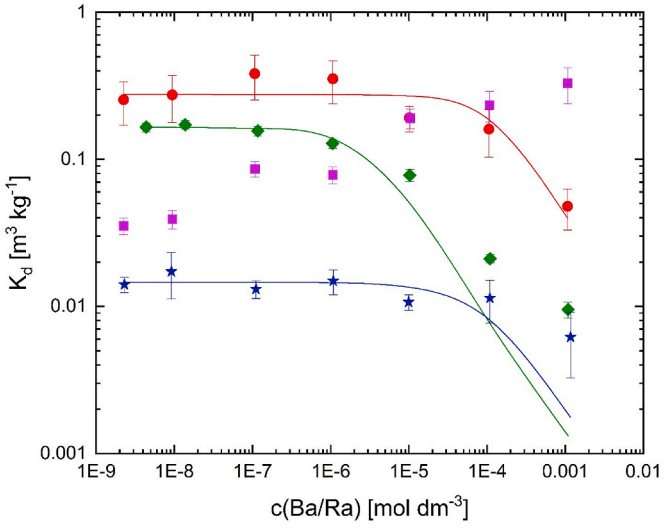

Fig. 3. Concentration dependent Ra sorption as experimental distribution coefficients on biotite in the fresh mildly reducing granitic ALLMR (●), fresh glacial meltwater OLGA (◆), sulfate and carbonate containing brackish OLBA (■), and saline reducing OLSR (★) reference groundwaters. Data points in the graph represent the averages of duplicate or triplicate samples. The curves (−) represent PHREEQC modeled data of the three experimental setups, color-coded respectively. (For interpretation of the references to color in this figure legend, the reader is referred to the Web version of this article.)

approximately one order of magnitude lower in the high Na^+, Mg^{2+}, and Ca^{2+} concentration saline OLSR than in the fresh ALLMR and OLGA. In the lower Ba concentrations (10^{-9} and 10^{-8} M) of OLBA, the experimental distribution coefficients of Ra in the mid-level salinity OLBA are situated between the fresh ALLMR and OLGA and the saline OLSR. This observation is consistent with the prediction of Ra distribution coefficient dependency on the salinity of the groundwater.

At the initial phase of the sorption model development, it was

Table 3
Best fit selectivity coefficients of sorption sites S_sOH (strong sites on FES), S_wOH (weak sites on cut surfaces), and ion exchange sites on mineral basal plane obtained with PHREEQC sorption modeling optimization in the reference groundwater conditions of ALLMR, OLGA, and OLSR.

Solution	K		
	S_sOH	S_wOH	Ion exchange
ALLMR	−5.20	−5.50	−9.55
OLGA	−5.85	−0.60	−4.85
OLSR	−3.72	−2.91	−2.59

suggested that the PHREEQC model for Ra and Ba sorption on biotite might underestimate the amount of sorption sites (or sorption site density) on the surface of biotite, thus overestimating the rate of sorption site saturation as the Ba isotherm concentration increases. The overestimation of the rate of saturation in the calculations would show as a premature and steeper decrease in the distribution coefficient trend. The DFT modeling results done in CASTEP were coupled into the PHREEQC models, updating the site densities of the sorption sites, remedying the model fitting issue noticeably. Additionally, according to thermodynamic calculations done with PHREEQC, in many of the experiments' higher Ba concentration conditions, the sorption solutions became well supersaturated in terms of barite and witherite. Thus, the fit of the models were further considerably improved with the inclusion of atmospheric CO_2 and Ba precipitation as barite and witherite balancing during the sorption reactions. As the coprecipitation of Ra with barite and witherite, in addition to sorption, has been estimated to have significant effect in the removal of Ra from aqueous solutions (Zhu, 2004; Grandia et al., 2008; Hedström et al., 2013; Yoshida et al., 2015; Matyskin, 2018), allowing the precipitation of Ba as barite and witherite during the sorption balancing was used to simulate the coprecipitation of Ra. As expected, the effect of precipitation on the model's Ba sorption was greatest in reference groundwater conditions with high amounts of sulfate and (bi)carbonate in them, namely ALLMR (SO_4^{2-}: 9.6 mg l^{-1}; HCO_3^-: 165 mg l^{-1}) and OLBA (SO_4^{2-}: 458 mg l^{-1}; HCO_3^-: 111 mg l^{-1}). The effect was, to a lesser extent, also visible in the modeling of OLGA and OLSR, reference groundwaters with no inherent carbonate and only meagre amounts added sulfate (0.2 mg l^{-1}, and 4.2 mg^{-1}, respectively). It is to be noted, however, that despite no carbonates were added during the preparation of OLGA and OLSR, the regular atmospheric conditions of the batch sorption experiments meant that dissolved CO_2 was bound to be present in all of the experimental conditions, thus affecting the precipitation balance of Ba as barite and witherite.

As a result of the modeling adjustments, the PHREEQC distribution coefficient models of the ALLMR, OLGA, and OLSR conditions are in good agreement with the experimental distribution coefficient results. Most notably, the model already agrees excellently with the

experimental results of ALLMR reference groundwater. In addition, especially in the lower to mid-level Ba isotherm concentrations (10^{-9} to 10^{-5} M), the model agrees very well with the experimental sorption results in the OLGA and OLSR reference groundwaters. Contrary to the other tested SGW conditions, the distribution coefficients of the reference groundwater OLBA even in the higher Ba isotherm concentration conditions (10^{-5} to 10^{-3} M) were discovered to increase when compared to the values at lower Ba concentrations. Based on thermodynamic calculations, the coprecipitation of Ra with barite and witherite was expected to increase the removal of Ra from the groundwater solutions. Especially in the case of OLBA, in the highest Ba concentration, the removal of Ra was calculated to be possibly as high as 100–150 Bq (of the spiked 200 Bq of ^{226}Ra), thus being a major competition for the sorption of Ra on biotite. Although the precipitation of Ba was used in the sorption model to simulate and compensate for the coprecipitation of Ra, the reason for the PHREEQC model's failure to fit the increasing trend of the experimental results of OLBA remains unresolved.

The tendency of coprecipitation of Ra with (Ba/Sr)SO_4 and corresponding carbonates will likely be a beneficial effect in the context of hindering the spread of radionuclides in the case of a nuclear waste containment breach in the deep geological disposal site (Grandia et al., 2008). As the Olkiluoto disposal site has a well-defined sulfate-rich layer of groundwater at the depth of 100–300 m, Ra and other sulfate (co) precipitating radionuclides stand to get retained in the layer, hindering the migration of the radionuclides on their way to biosphere. Despite this, in natural undisturbed groundwater conditions, where the concentrations of Ba and Ra are generally very low (Vaaramaa et al., 2003; Ervanne et al., 2014), the coprecipitation of Ra poses little effect for the migration of said element.

4. Conclusions

The distribution coefficients of Ra on biotite in four different types of reference groundwaters were studied in the presence of Ba concentration isotherm as an analog to Ra. In three of the four studied reference groundwaters, the experimental distribution coefficients were found to be well within predictions and similar with previous studies with Ra (Söderlund et al., 2019), with the sorption of Ra decreasing in sorption conditions of higher salinity and ionic competition. The distribution coefficients were largest in reference groundwater conditions of low salinity and low Ba isotherm concentration (10^{-9} M): in the fresh ALLMR and OLGA reference groundwaters the distribution coefficients of Ra were 0.25 ± 0.09 m^3 kg^{-1} and 0.17 ± 0.02 m^3 kg^{-1}, respectively. In the saline reference groundwater OLSR, even in the low isotherm concentration (10^{-9} M), the distribution coefficient of Ra was one order of magnitude lower than in the fresh reference groundwaters: 0.014 ± 0.002 m^3 kg^{-1}. Both in the fresh reference groundwaters, ALLMR and OLGA, and in the saline OLSR, the sorption and distribution coefficients of Ra were significantly lower in conditions of high Ba concentration (10^{-3} M): 0.048 ± 0.020 m^3 kg^{-1}, 0.010 ± 0.002 m^3 kg^{-1}, and 0.006 ± 0.003 m^3 kg^{-1}, respectively. Most of the experimental results of the sorption of Ra on biotite were found to agree well with the multi-site model outlined by Bradbury and Bayens (2000). However, the experimental results of the final SGW, the sulfate and carbonate containing brackish OLBA, were found to disagree with the sorption model. With OLBA, in contrast to the other three reference groundwaters, the calculated distribution coefficients of Ra were lower in the low Ba concentrations (0.035 ± 0.005 m^3 kg^{-1} in 10^{-9} M) than in the high Ba concentrations (0.33 ± 0.09 m^3 kg^{-1} in 10^{-3} M). With PHREEQC thermodynamic calculations, it was concluded that the significant amounts of SO_4^{2-} and HCO_3^- (458 mg l^{-1}, and 111 mg l^{-1}, respectively) of OLBA in higher Ba isotherm concentrations encourage coprecipitation of Ra with Ba as (Ba,Ra)SO_4 and (Ba,Ra)CO_3, removing free Ra from the sorption supernatant and showing an increase in the calculated distribution coefficients. The same effect of Ra coprecipitation on the experimental distribution coefficients was observed in the calculations and modeling of other reference groundwaters, as well, but to a lesser extent.

To support and interpret the experimental Ra sorption results, a PHREEQC sorption model was developed based on the Bradbury and Bayens multi-site sorption model. In the initial phase of the modeling work, DFT modeling was used to update the PHREEQC model with more realistic sorption site density data: 5.6 strong sites nm^{-2} and 5.6 weak sites nm^{-2} on the mineral sheet edges and 4.2 sites nm^{-2} on the basal site of the mineral. In addition to this, the PHREEQC model was adjusted with the inclusion of barite and witherite precipitation to simulate the well-established tendency of Ra to coprecipitate with Ba. The more realistic sorption site density and precipitation data improved the fit of the PHREEQC models considerably. For the fresh reference groundwater ALLMR, OLGA, and the saline OLSR, the PHREEQC model fitted very well the experimental Ra distribution coefficient results. It was observed, however, that in the higher Ba isotherm concentrations (10^{-3} M) the modeled distribution coefficients (0.001 m^3 kg^{-1} and 0.002 m^3 kg^{-1} in 10^{-3} M for OLGA and OLSR, respectively) tended to decrease somewhat more sharply than the corresponding experimental values suggested. For the brackish reference groundwater OLBA, the precipitation fix of the model improved the fit to experimental results only moderately. To further investigate the sorption mechanism of Ra in the context of deep geological disposal, sorption and site mechanism experiments and modeling on crystalline whole rocks and different groundwater conditions will be conducted in the future.

Author's contributions

O. Fabritius and M. Siitari-Kauppi conceived the research. O. Fabritius conducted all the experiments with the help of A. Nurminen. E. Puhakka performed the DFT modeling while O. Fabritius and X. Li performed the experimental data modeling together. O. Fabritius and E. Puhakka wrote the manuscript. M. Siitari-Kauppi and X. Li supervised the working process and commented on the manuscript.

All authors have approved the final manuscript.

Declaration of competing interest

The authors declare that they have no known competing financial interests or personal relationships that could have appeared to influence the work reported in this paper.

Acknowledgments

The project leading to this work has received funding from the European Union's Horizon 2020 research and innovation program under grant agreement No. 847593. This work was supported by the Finnish nuclear waste disposal company Posiva Oy. The authors wish to acknowledge CSC – IT Center for Science, Finland, for computational resources. We wish to thank Stellan Holgersson of the Chalmers University of Technology for the biotite BET/SSA analysis, and Lauri Parviainen and Petteri Pitkänen of Posiva for the valuable comments on the manuscript.

References

Aaltonen, I., Engström, J., Front, K., Gehör, S., Kosunen, P., Kärki, A., Paananen, M., Paulamäki, S., Mattila, M., 2016. Geology of Olkiluoto (POSIVA 2016-16). Posiva Oy.

Appelo, C.A.J., Postma, D., 2005. Geochemistry, Groundwater and Pollution, second ed. A.A. Balkema Publishers, Amsterdam. https://doi.org/10.1201/9781439833544.

Armarego, W.L.F., Chai, C.L.L., 2012. Purification of Laboratory Chemicals, seventh ed. Butterworth-Heinemann, Oxford.

Aromaa, H., Voutilainen, M., Ikonen, J., Yli-Kaila, M., Poteri, A., Siitari-Kauppi, M., 2019. Through diffusion experiments to study the diffusion and sorption of HTO, ^{36}Cl, ^{133}Ba and ^{134}Cs in crystalline rock. J. Contam. Hydrol. 222, 101–111. https://doi.org/10.1016/j.jconhyd.2019.03.002.

Bradbury, M.H., Bayens, B., 2000. A generalized sorption model for the concentration dependent uptake of cesium by argillaceous rocks. J. Contam. Hydrol. 42, 141–163. https://doi.org/10.1016/S0169-7722(99)00094-7.

Breitner, D., Turtiainen, T., Arvela, H., Vesterbacka, P., Johanson, B., Lehtonen, M., Hellmuth, K.-H., Szabó, C., 2008. Multidisciplinary analysis of Finnish esker sediment in radon source identification. Sci. Total Environ. 405, 129–139. https://doi.org/10.1016/j.scitotenv.2008.06.015.

Charlton, S.R., Parkhurst, D.L., 2011. Modules based on the geochemical model PHREEQC for use in scripting and programming languages. Comput. Geosci. 37–10, 1653–1663. https://doi.org/10.1016/j.cageo.2011.02.005.

Crawford, J., 2010. Bedrock K_d Data and Uncertainty Assessment for Application in SR-Site Geosphere Transport Calculations (SKB R-10-48). Svensk Kärnbränslehantering AB.

Davis, S.N., 1964. In: Krieger, R.A. (Ed.), The Chemistry of Saline Waters, vols. 2–1, p. 51. Discussion. Groundwater.

Déjeant, A., Bourva, L., Sia, R., Galoisy, L., Calas, G., Phrommavanh, V., Descostes, M., 2014. Field analyses of 238U and 226Ra in two uranium mill tailings piles from Niger using portable HPGe detector. J. Environ. Radioact. 137, 105–112. https://doi.org/10.1016/j.jenvrad.2014.06.012.

Dzombak, D., Morel, F., 1990. Surface Complexation Modeling: Hydrous Ferric Oxide. John Wiley & Sons, New York.

Ervanne, H.J., Puukko, E.J., Hakanen, M.E., 2013. Modeling of Sorption of Eu, Mo, Nb, Ni, Pa, Se, Sn, Th and U on Kaolinite and Illite in Olkiluoto Groundwater Simulants (POSIVA 2013-31). Posiva Oy.

Ervanne, H.J., Hakanen, M.E., Puukko, E.J., 2014. Safety Case for the Disposal of Spent Nuclear Fuel at Olkiluoto (POSIVA 2012-41). Posiva Oy.

Ewing, R.C., 2015. Long-term storage of spent nuclear fuel. Nat. Mater. 14, 252–257. https://doi.org/10.1038/nmat4226.

Grandia, F., Merino, J., Bruno, J., 2008. Assessment of the Radium-Barium Co-precipitation and its Potential Influence on the Solubility of Ra in the Near-Field (SKB TR-08-07). Svensk Kärnbränslehantering AB.

Greeman, D.J., Rose, A.W., Washington, J.W., Dobos, R.R., Ciolkosz, E.J., 1999. Geochemistry of radium in soils of the Eastern United States. Appl. Geochem. 14–3, 365–385. https://doi.org/10.1016/S0883-2927(98)00059-6.

Hedström, H., Ramebäck, H., Ekberg, C., 2013. A study of the Arrhenius behavior of the co-precipitation of radium, barium and strontium sulfate. J. Radioanal. Nucl. Chem. 298, 847–852. https://doi.org/10.1007/s10967-013-2431-0.

Hellä, P., Pitkänen, P., Löfman, J., Partamies, S., Vuorinen, U., Wersin, P., 2014. Safety Case for the Disposal of Spent Nuclear Fuel at Olkiluoto - Definition of Reference and Bounding Groundwaters, Buffer and Backfill Porewaters (POSIVA 2014-04). Posiva Oy.

Huitti, T., Hakanen, M., Lindberg, A., 1996. Sorption of Cesium, Radium, Protactinium, Uranium, Neptunium and Plutonium on Rapakivi Granite (POSIVA 1996-23). Posiva Oy.

International Atomic Energy Agency, 2004. Treatment of Liquid Effluent from Uranium Mines and Mills. IAEA, Vienna, Austria.

International Atomic Energy Agency, 2014. The Environmental Behaviour of Radium, revised edition. IAEA, Vienna, Austria.

Jaremalm, M., Köhler, S., Lidman, F., 2013. Precipitation of Barite in the Biosphere and its Consequences for the Mobility of Ra in Forsmark and Simpevarp (SKB TR-13-28). Svensk Kärnbränslehantering AB.

Jonsson, M., Emilsson, G., Emilsson, L., 2018. Mechanical Design Analysis for the Canister (POSIVA-SKB 04). Posiva Oy & Svensk Kärnbränslehantering AB.

Kärki, A., Paulamäki, S., 2006. Petrology of Olkiluoto (POSIVA 2006-02). Posiva Oy.

Kuva, J., 2016. Tracer Migration in Crystalline Rock - Application to Geological Barriers of Nuclear Waste Storage. PhD thesis. University of Jyväskylä.

Kuva, J., Siitari-Kauppi, M., Lindberg, A., Aaltonen, I., Turpeinen, T., Myllys, M., Timonen, J., 2012. Microstructure, porosity and mineralogy around fractures in Olkiluoto bedrock. Eng. Geol. 139–140, 28–37. https://doi.org/10.1016/j.enggeo.2012.04.008.

Lehto, J., Hou, X., 2011. Chemistry and Analysis of Radionuclides. Wiley-VCH, Weinheim, Germany.

Li, X., Puhakka, E., Ikonen, J., Söderlund, M., Lindberg, A., Holgersson, S., Martin, A., Siitari-Kauppi, M., 2018. Sorption of Se species on mineral surfaces, part I: batch sorption and multi-site modelling. Appl. Geochem. 95, 147–157. https://doi.org/10.1016/j.apgeochem.2018.05.024.

Li, X., Puhakka, E., Liu, L., Zhang, W., Ikonen, J., Lindberg, A., Siitari-Kauppi, M., 2020. Multi-site surface complexation modelling of Se(IV) sorption on biotite. Chem. Geol. 533, 119433. https://doi.org/10.1016/j.chemgeo.2019.119433.

Lindberg, A., 2001. Biotiitin Pysyvyys Olkiluodon Loppusijoitusolosuhteissa – Kirjallisuusselvitys (POSIVA 2001-12). Posiva Oy.

Liu, L., Neretnieks, I., Shahkarami, P., Meng, S., Moreno, L., 2018. Solute transport along a single fracture in a porous rock: a simple analytical solution and its extension for modeling velocity dispersion. Hydrogeol. J. 26, 297–320. https://doi.org/10.1007/s10040-017-1627-8.

Mäki, J.-M., 2021. Safety Case for the Operating Licence Application: Modelling Report for Simplified Landscape Dose Conversion Model (POSIVA 2021-23). Posiva Oy.

Martin, A.J., Crusius, J., McNee, J.J., Yanful, E.K., 2003. The mobility of radium-226 and trace metals in pre-oxidized subaqueous uranium mill tailings. Appl. Geochem. 18–7, 1095–1110. https://doi.org/10.1016/S0883-2927(02)00243-3.

Matyskin, A.V., 2018. Solubility and Crystal Structure of Radium Sulfate and Carbonate. PhD thesis. Chalmers University of Technology.

Matyskin, A.V., Ylmen, R., Lagerkvist, P., Ramebäck, H., Ekberg, C., 2017. Crystal structure of radium sulfate: an X-ray powder diffraction and density functional theory study. J. Solid State Chem. 253, 15–20. https://doi.org/10.1016/j.jssc.2017.05.024.

Missana, T., Colàs, E., Grandia, F., Olmeda, J., Mingarro, M., García-Gutiérrez, M., Munier, I., Robinet, J.-C., Grivé, M., 2017. Sorption of radium onto early cretaceous clays (Gault and Plicatules Fm). Implications for a repository of low-level, long-lived radioactive waste. Appl. Geochem. 86, 36–48. https://doi.org/10.1016/j.apgeochem.2017.09.009.

Muikku, M., Bly, R., Kurttio, P., Lahtinen, J., Lehtinen, M., Siiskonen, T., Turtiainen, T., Valmari, T., Vesterbacka, K., 2014. Suomalaisten Keskimääräinen Efektiivinen Annos; Annoskakku 2012 (STUK-A259). Finnish Radiation and Nuclear Safety Authority (STUK).

Muuri, E., Ikonen, J., Matara-aho, M., Lindberg, A., Holgersson, S., Voutilainen, M., Siitari-Kauppi, M., Martin, A., 2016. Behavior of Cs in Grimsel granodiorite: sorption on main minerals and crushed rock. Radiochim. Acta 104, 575–582. https://doi.org/10.1515/ract-2015-2574.

Muuri, E., Siitari-Kauppi, M., Matara-Aho, M., Ikonen, J., Lindberg, A., Qian, L., Koskinen, L., 2017. Cesium sorption and diffusion on crystalline rock: Olkiluoto case study. J. Radioanal. Nucl. Chem. 311, 439–446. https://doi.org/10.1016/j.heliyon.2019.e02296.

Muuri, E., Matara-aho, M., Puhakka, E., Ikonen, J., Siitari-Kauppi, M., Martin, A., Koskinen, L., 2018. The sorption and diffusion of ^{133}Ba in crushed and intact granitic rocks from the Olkiluoto and Grimsel in-situ test sites. Appl. Geochem. 89, 138–149. https://doi.org/10.1016/j.apgeochem.2017.12.004.

Neretnieks, I., 2013. Some aspects of release and transport of gases in deep granitic rocks: possible implications for nuclear waste repositories. Hydrogeol. J. 21, 1701–1716. https://doi.org/10.1007/s10040-013-0986-z.

Neretnieks, I., Winberg-Wang, H., 2019. Density-driven mass transfer in repositories for nuclear waste. Nucl. Technol. 205, 819–829. https://doi.org/10.1080/00295450.2018.1537460.

Olmeda, J., Missana, T., Grandia, F., Grivé, M., García-Gutiérrez, M., Mingarro, M., Alonso, U., Colàs, E., Henocq, P., Munier, I., Robinet, J.-C., 2019. Radium retention by blended cement pastes and pure phases (C-S-H and C-A-S-H gels): experimental assessment and modelling exercises. Appl. Geochem. 105, 45–54. https://doi.org/10.1016/j.apgeochem.2019.04.004.

Parkhurst, D.L., Appelo, C.A.J., 2013. Description of Input and Examples for PHREEQC Version 3: a Computer Program for Speciation, Batch-Reaction, One-Dimensional Transport, and Inverse Geochemical Calculations (U.S. Geological Survey Techniques and Methods Report 6-A43). Reston, Virginia.

Partamies, S., Pitkänen, P., 2014. Mass-Balance Modelling Results of Groundwater Data Collected at Olkiluoto over the Period 2004-2007 (POSIVA 2014-06). Posiva Oy.

Posiva, 1996. Käytetyn Polttoaineen Loppusijoitus Suomen Kallioperään; Paikkakohtaisen Turvallisuusanalyysin Edellytykset Ja Mahdollisuudet (POSIVA 1996-16). Posiva Oy.

Posiva, 2012a. Safety Case for the Disposal of Spent Nuclear Fuel at Olkiluoto - Complementary Considerations 2012 (POSIVA 2012-11). Posiva Oy.

Posiva, 2012b. Safety Case for the Disposal of Spent Nuclear Fuel at Olkiluoto - Synthesis 2012 (POSIVA 2012-12). Posiva Oy.

Posiva, 2012c. Olkiluoto Site Description 2011 (POSIVA 2011-02). Posiva Oy.

Posiva, 2013. Safety Case for the Disposal of Spent Nuclear Fuel at Olkiluoto; Models and Data for the Repository System 2012 (POSIVA 2013-01). Posiva Oy.

Posiva, 2017. Safety Case Plan for the Operating Licence Application (POSIVA 2017-02). Posiva Oy.

Posiva, 2021. Source Terms for the Safety Case in Support of the Operating License Application (POSIVA 2021-11). Posiva Oy.

Sajih, M., Bryan, N.D., Livens, F.R., Vaughan, D.J., Descostes, M., Phrommavanh, V., Nos, J., Morris, K., 2014. Adsorption of radium and barium on goethite and ferrihydrite: a kinetic and surface complexation modelling study. Geochem. Cosmochim. Acta 146, 150–163. https://doi.org/10.1016/j.gca.2014.10.008.

Sammaljärvi, J., Lindberg, A., Voutilainen, M., Ikonen, J., Siitari-Kauppi, M., Pitkänen, P., Koskinen, L., 2017. Multi-scale study of the mineral porosity of veined gneiss and pegmatitic granite from Olkiluoto, Western Finland. J. Radioanal. Nucl. Chem. 314, 1557–1575. https://doi.org/10.1007/s10967-017-5530-5.

Shahkarami, P., Liu, L., Moreno, L., Neretnieks, I., 2015. Radionuclide migration through fractured rock for arbitrary-length decay chain: analytical solution and global sensitivity analysis. J. Hydrol. 520, 448–460. https://doi.org/10.1016/j.jhydrol.2014.10.060.

Shannon, R.T., 1976. Revised effective ionic radii and systematic studies of interatomic distances in halides and chalcogenides. Acta Crystallogr. 32, 751–767. https://doi.org/10.1107/S0567739476001551.

SKB, 2006. Long-term Safety for KBS-3 Repositories at Forsmark and Laxemar - a First Evaluation (SKB TR-06-09). Svensk Kärnbränslehantering AB.

Söderlund, M., Ervanne, H., Muuri, E., Lehto, J., 2019. The sorption of alkaline earth metals on biotite. Geochem. J. 53, 223–234. https://doi.org/10.2343/geochemj.2.0561.

BIOVIA, Systèmes, Dassault, 2019. Materials Studio 2020. Dassault Systèmes, San Diego.

Tsang, C.-F., Neretnieks, I., Tsang, Y., 2015. Hydrologic issues associated with nuclear waste repositories. Water Resour. Res. 51–9, 6923–6972. https://doi.org/10.1002/2015WR017641.

Vaaramaa, K., Lehto, J., Ervanne, H., 2003. Soluble and particle-bound 234,238U, 226Ra and 210Po in ground waters. Radiochim. Acta 91, 21–27. https://doi.org/10.1524/ract.91.1.21.19015.

Velde, B., Meunier, A., 2008. The Origin of Clay Minerals in Soils and Weathered Rocks. Springer-Verlag, Berlin, Heidelberg.

Viani, A., Gualtieri, A.F., Artioli, G., 2002. The nature of disorder in montmorillonite by simulation of X-ray powder patterns. Am. Mineral. 87, 966–975. https://doi.org/10.2138/am-2002-0720.

Vieno, T., 2000. Groundwater Salinity at Olkiluoto and its Effects on a Spent Fuel Repository (POSIVA 2000-11). Posiva Oy.

Vinograd, V.L., Kulik, D.A., Brandt, F., Klinkenberg, M., Weber, J., Winkler, B., Bosbach, D., 2018. Thermodynamics of the solid solution - aqueous solution system (Ba,Sr,Ra)SO4 + H2O. The effect of strontium content on radium uptake by barite. Appl. Geochem. 89, 59–74. https://doi.org/10.1016/j.apgeochem.2017.11.009.

Voutilainen, M., Ikonen, J., Sammaljärvi, J., Kuva, J., Lindberg, A., Siitari-Kauppi, M., Koskinen, L., 2016. Through diffusion study on Olkiluoto veined gneiss and pegmatitic granite from a structural perspective. MRS Adv. 1–61, 4041–4046. https://doi.org/10.1557/adv.2017.187.

Voutilainen, M., Ikonen, J., Sammaljärvi, J., Siitari-Kauppi, M., Lindberg, A., Kuva, J., Timonen, J., Löfgren, M., 2018. Investigation of Rock Matrix Retention Properties - Supporting Laboratory Studies II: Diffusion Coefficient and Permeability (POSIVA 2017-39). Posiva Oy.

Voutilainen, M., Kekäläinen, P., Poteri, A., Siitari-Kauppi, M., Helariutta, K., Andersson, P., Nilsson, K., Byegård, J., Skålberg, M., Yli-Kaila, M., Koskinen, L., 2019. Comparison of water phase diffusion experiments in laboratory and in situ conditions. J. Hydrol. 575, 716–729. https://doi.org/10.1016/j.jhydrol.2019.05.069.

Vuorinen, U., Snellman, M., 1998. Finnish Reference Waters for Solubility, Sorption and Diffusion Studies (POSIVA 1998-61). Posiva Oy.

Wissmeier, L., Barry, D.A., 2011. Simulating tool for variably saturated flow with comprehensive geochemical reactions in two- and three-dimensional domains. Environ. Model. Software 26–2, 210–218. https://doi.org/10.1016/j.envsoft.2010.07.005.

Yoshida, Y., Nakazawa, T., Yoshikawa, H., 2015. Partition coefficient of Ra in witherite. J. Radioanal. Nucl. Chem. 303, 147–152. https://doi.org/10.1007/s10967-014-3357-x.

Zhu, C., 2004. Coprecipitation in the barite isostructural family: 2. Numerical simulations of reactions and mass transport. Geochem. Cosmochim. Acta 68–16, 3339–3349. https://doi.org/10.1016/j.gca.2003.10.013.